Slow sites in an exclusion process with limited resources

Chris A. Brackley,[1] M. Carmen Romano,[2,1] and Marco Thiel[1]
[1]*Institute for Complex Systems and Mathematical Biology, SUPA, University of Aberdeen, Aberdeen AB24 3UE, United Kingdom*
[2]*Institute of Medical Sciences, Foresterhill, University of Aberdeen, Aberdeen AB25 2ZD, United Kingdom*
(Received 22 July 2010; revised manuscript received 23 September 2010; published 17 November 2010)

We introduce slow bottleneck sites into a recent extension of the totally asymmetric exclusion process where hopping rates are allowed to vary dynamically with the availability of resources. In the context of messenger RNA (mRNA) translation in biology, this refers to the availability of amino acid-transfer-RNA (aa-tRNA) complexes which act as the source of amino acids for protein production. We study a simple designer mRNA with a single defect codon in the center. As well as the familiar queuing behavior we also observe a regime within the queuing phase where the queue becomes less severe as the aa-tRNAs become depleted.

DOI: 10.1103/PhysRevE.82.051920 PACS number(s): 87.10.−e, 05.45.−a

I. INTRODUCTION

In this paper we study a driven diffusion model of messenger RNA (mRNA) translation in which the particle current depends both on the availability of resources and the propensity of particles to queue behind slow bottleneck sites. Translation is part of the cellular process of protein production [1]. Similar in structure to DNA, mRNA molecules are sequences of codons which encode the amino acid sequences which make up proteins. Each codon consists of three nucleotides of which there are four types. Proteins are assembled by molecular machines called ribosomes, which move along the mRNA in a stepwise manner, reading the codons and adding relevant amino acids to a growing peptide chain. Understanding the translation process is a key factor in answering questions about how a cell selects which proteins it will produce and how this production is affected by changes in the environment.

A popular model which can be applied to translation, as well as many other systems (e.g., traffic flow [2] or intracellular transport via molecular motors [3]), is the totally asymmetric exclusion process (TASEP) [4]. As one of the archetypal models of nonequilibrium statistical mechanics, the TASEP consists of a one-dimensional (1D) lattice of discrete sites and particles which hop between these sites. Only a single particle can occupy a site, and particles hop in one direction only, entering the lattice at the left and leaving it at the right. Clearly a nonequilibrium process, the TASEP exhibits rich dynamics showing multiple phases. The system is characterized by the particle current J and mean particle density $\bar{\rho}$ which are functions of the rates at which particles hop onto, along, and off of the lattice. In some parameter regimes it is possible to calculate the stationary state current and densities exactly, while more generally a mean-field model (where spatial correlations are neglected) accurately describes the system [5–7]. For modeling translation, the sites of the lattice represent the codons of the mRNA, and the particles represent the ribosomes.

In addition to the mRNA and ribosomes, a third important part of translation is the delivery of amino acids to the ribosome by transfer RNA (tRNA) molecules, which are different for different types of codons. It is thought that the rate at which a ribosome translates a given codon depends on the abundance of the relevant tRNA molecule [8,9], i.e., codons which code for a low abundance tRNA will be translated at a much slower rate. We call these "slow codons." With a code of four different nucleotides there are 64 possible codons; there are, however, only 20 common amino acids which are carried by 41 species of tRNA. This means that the code can be redundant: there is more than one possible codon sequence for a particular protein. Much work has focused on the fact that for reasons not fully understood, some mRNA sequences contain slow codons when there exist alternate tRNAs which carry the same amino acid and are much more abundant. There have been many suggestions as to the possible advantages of such sequences. It could be that slow codons provide pauses in translation, giving time for proteins to fold in a specific way [10]. It could give further (to transcriptional) control over protein production rates and allow fast response to changes in environmental conditions [11]. Or perhaps different classes of mRNAs have different patterns of slow codon usage in order to give them specific translational properties [12]. The TASEP has been used to assay the effect of slow codons on the protein production mechanism and to help answering some of these questions. For example Chou and Lakatos [13] looked at the effect of clusters of several slow codons, Dong *et al.* [14] studied the effect of changing the separation and proximity to the initiation end of the mRNA of a pair of slow codons, and Romano *et al.* [12] identified a correlation between the functional properties of mRNAs and the position of the slowest codon.

A recent study [15] includes in the TASEP model the fact that the number of amino acid tRNA (aa-tRNA) complexes in the cell is dynamic. When an amino acid is added to the peptide chain a bare tRNA molecule is left; while tRNAs are not used up in the process it takes a finite time for them to be "recharged" with a new amino acid. The model considers finite tRNA resources, in contrast to other recent work [16–18] which examines the effect of finite resources of a different type, namely, the availability of ribosomes. In this paper we extend the model with finite tRNA recharging to include slowly translated codons which act as bottlenecks and can lead to queuing of ribosomes. In the next section we briefly discuss previous results for a TASEP with a slow site, and then review our model for finite aa-tRNA recharging. Section III describes a mean-field model of a TASEP with both finite aa-tRNA recharging *and* a slow codon and compares this with Monte Carlo simulations (MCSs).

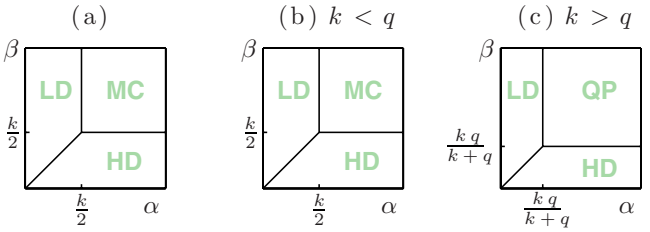

FIG. 1. (Color online) (a) Phase plane for the original TASEP with a uniform lattice, showing the LD, HD, and MC phases. Plots (b) and (c) show phase places for the TASEP with a single defect site in the center of the lattice. In (b), where $k<q$, the defect site has no effect on the phase plane and LD, HD, and MC phases exist. In (c), where $k>q$, at large α,β the MC phase is replaced with a queuing phase. We note that as q is increased the QP region reduces in size until $q=k$, where we recover the plot in (b).

II. REVIEW OF PREVIOUS RESULTS

A. TASEP

The TASEP [4–7,19,20] consists of a 1D lattice of length L sites. We define the occupation n_i of the ith site as being 0 if the site is vacant and 1 if it contains a particle. Particles hop onto the lattice at the left with rate α, leave the lattice at the right with rate β, and hop along the lattice with site-dependent rate k_i. We term the ensemble average occupancy of the sites the particle density ρ_i and assume that the system is ergodic, so that at steady state $\rho_i=\langle n_i\rangle_t$, where $\langle\cdots\rangle_t$ denotes time average. The system is characterized by the mean density $\bar{\rho}=L^{-1}\Sigma_i\rho_i$, and the particle current J which also corresponds to the protein production rate.

For simplicity we first look at a very simple "designer mRNA," in which all codons are the same, i.e., $k_i=k\ \ \forall i$. By assuming that there are no spatial correlations between the occupation probabilities of different sites, one can write mean-field equations describing the dynamics of the density at each site as

$$\frac{d\rho_1}{dt} = \alpha(1-\rho_1) - k\rho_1(1-\rho_2),$$

$$\frac{d\rho_L}{dt} = k\rho_{L-1}(1-\rho_L) - \beta\rho_L,$$

$$\frac{d\rho_i}{dt} = k\rho_{i-1}(1-\rho_i) - k\rho_i(1-\rho_{i+1}), \quad i=2,\ldots,L-1. \tag{1}$$

In steady state, where we identify the current

$$J = k\rho_i(1-\rho_{i+1}), \tag{2}$$

independent of i, we find that the system can exist in several phases depending on the relative magnitudes of the parameters α, β, and k [5–7]. There are low-density (LD) and high-density (HD) phases (entry and exit limited phases) and a maximal current (MC) phase where the current J reaches its maximum value limited by the steric interactions between the particles. The phase diagram is shown in Fig. 1(a), and the phases can be summarized as follows:

$$\text{LD: } J=\alpha\left(1-\frac{\alpha}{k}\right), \quad \rho=\frac{\alpha}{k}, \quad \alpha<\beta, \alpha\le\frac{k}{2},$$

$$\text{HD: } J=\beta\left(1-\frac{\beta}{k}\right), \quad \rho=\frac{1-\beta}{k}, \quad \beta<\alpha, \beta\le\frac{k}{2},$$

$$\text{MC: } J=\frac{k}{4}, \quad \rho=\frac{1}{2}, \quad \alpha,\beta>\frac{k}{2}, \tag{3}$$

where ρ gives the density of sites in the bulk. Although ρ_i deviates from ρ near sites 0 and L due to edge effects (spatial correlations in the density), if L is sufficiently large we can approximate $\rho\approx\bar{\rho}$. A mixed LD-HD or shock phase is found for $\alpha=\beta\le k/2$, and this has been studied extensively elsewhere [19,21]. In many previous works, authors took $k=1$ and treated α as a hopping probability. Since in Sec. II C we will allow the hopping rate to vary as a function of the number of available charged tRNAs, it is necessary to keep k explicitly in these equations. One can consider the probability $\alpha\Delta t$ of an initiation event occurring in time Δt, but here we use continuous time.

B. TASEP with a slow site

In order to understand the effect of slow codons on translation, several authors [13,22–27] have studied slightly more complicated designer mRNAs with one or more slow codons. For example a very simple case is where all codons are the same except the one in the very center of the lattice; i.e., $k_i=k$ for $i\neq L/2$, and $k_{L/2}=q$. We can define the relative speed of the central codon as

$$s=\frac{q}{k}.$$

This system is studied in [27] by Kolomeisky, who assumed that the lattice can be modeled as two separate sublattices connected across the slow site. The leftmost lattice has entry and exit rates α and β_{eff}, and the rightmost α_{eff} and β, respectively, where

$$\beta_{\text{eff}}=q(1-\rho_{L/2+1}), \quad \alpha_{\text{eff}}=\rho_{L/2}q. \tag{4}$$

Noting that $J=q\rho_{L/2}(1-\rho_{L/2+1})$, the current can also be expressed as

$$J=\frac{\alpha_{\text{eff}}\beta_{\text{eff}}}{q}. \tag{5}$$

Assuming that the different sublattices can exist in the same phases as the uniform TASEP, there are four possible phases for the combined system: LD/LD, HD/HD, MC/MC, and HD/LD [28]. The HD/LD phase can be described as a queue of particles behind the slow codon, and we hereon denote it the queuing phase (QP).

As one would expect, when the two sublattices are in the same phase the behavior is the same as in the uniform TASEP. Following Eqs. (3), for LD/LD we have

$J=\alpha(1-\alpha/k)$ for the leftmost sublattice, but also $J=\alpha_{\text{eff}}(1-\alpha_{\text{eff}}/k)$ to the right of the slow codon. Equating these currents, since in steady state the current must be constant throughout the lattice, and taking into consideration the definition of α_{eff} [Eq. (4)] leads to $\alpha_{\text{eff}}=\alpha$. Using Eq. (5) then leads to $\beta_{\text{eff}}=q(1-\alpha/k)$. Considering the inequalities for LD given in Eqs. (3) for both sublattices gives $\alpha<\beta_{\text{eff}}$, $\alpha_{\text{eff}}<\beta$, and $\alpha,\alpha_{\text{eff}}\leq k/2$; eliminating α_{eff} and β_{eff} gives

$$\text{LD:}\quad \left.\begin{aligned} J&=\alpha\left(1-\frac{\alpha}{k}\right)\\ \rho&=\frac{\alpha}{k}\end{aligned}\right\}\quad \text{for}\quad \begin{aligned}&\alpha<\beta\\ &\alpha\leq\frac{k}{2}\\ &\alpha<\frac{qk}{k+q},\end{aligned} \tag{6}$$

i.e., as well as conditions on α and β we now have a condition on q. Equivalent results for the HD/HD phase can be found easily due to particle-hole symmetry. For the MC/MC phase we have from Eq. (3) the current $J=k/4$ and the inequalities $\alpha,\beta,\alpha_{\text{eff}},\beta_{\text{eff}}>k/2$. Although α_{eff} and β_{eff} are not defined independently in this phase, from the inequalities we can infer that $\alpha_{\text{eff}}\beta_{\text{eff}}>k^2/4$, and using Eq. (5) gives

$$\text{MC:}\quad \left.\begin{aligned} J&=\frac{k}{4}\\ \rho&=\frac{1}{2}\end{aligned}\right\}\quad \text{for}\quad \begin{aligned}&\alpha,\beta>\frac{k}{2}\\ &q>k.\end{aligned} \tag{7}$$

This means that we can only reach the MC phase if the defect codon is "faster" than the other codons. If in contrast, the defect codon is slower than the others, we reach the QP (HD/LD phase). The leftmost sublattice obeys the HD equations in Eqs. (3) and the rightmost half obeys the LD equations. That is, $J=\alpha_{\text{eff}}(1-\alpha_{\text{eff}}/k)$ and $J=\beta_{\text{eff}}(1-\beta_{\text{eff}}/k)$; equating again gives two solutions for α_{eff} and β_{eff}, with the only physical one being $\alpha_{\text{eff}}=\beta_{\text{eff}}$.

Together with the inequalities $\alpha_{\text{eff}}<\beta$, $\beta_{\text{eff}}<\alpha$, and $\alpha_{\text{eff}},\beta_{\text{eff}}\leq k/2$, this gives the full solution for the QP,

$$\text{QP:}\quad \left.\begin{aligned} J&=\frac{k^2q}{(k+q)^2}\\ \rho_l&=\frac{k}{k+q}\\ \rho_r&=\frac{q}{k+q}\end{aligned}\right\}\quad \text{for}\quad \begin{aligned}&q<k\\ &\alpha>\frac{kq}{k+q}\\ &\beta>\frac{kq}{k+q},\end{aligned} \tag{8}$$

where ρ_l (ρ_r) is the bulk density to the left (right) of the slow site. The queuing phase can be identified by a nonzero value of $\Delta\rho=\rho_l-\rho_r$, which is found to be

$$\Delta\rho=\frac{1-s}{1+s}.$$

Figure 1(b) shows the phase plane for the TASEP with a defect site which is faster than the other codons, and Fig. 1(c) shows the same for a defect which is slower than the other codons.

Kolomeisky [27] used this simple mean-field approach to predict the presence of the QP. This approach yields qualitatively good results; however, since the slow site introduces significant spatial correlations in the occupation probabilities, the mean-field approximation does not exactly predict the densities or current. This becomes apparent for small L, when Monte Carlo simulations begin to significantly deviate from the mean-field results (not shown). Chou and Lakatos [13] proposed a more accurate treatment, where the densities and effective hopping rates of a region of n sites around the slow site j are considered; they find that $n\sim 3$ is sufficient to accurately predict the currents. Since this method relies on the numerical calculation of a $2^n\times 2^n$ transition matrix, it is not straightforward to incorporate finite tRNA charging via an analytical treatment. We therefore follow the method of Kolomeisky throughout this paper.

C. TASEP with finite aa-tRNA recharging rate

We recently detailed an extension to the TASEP for a uniform ($k_i=k\ \forall i$) mRNA where the hopping rate k is allowed to vary with the availability of resources [15]. There is a pool of charged aa-tRNAs and a pool of uncharged tRNAs; every time a particle hops along the lattice we reduce the aa-tRNA pool by 1 and increase the tRNA pool correspondingly. We model a system of N mRNAs connected to the same tRNA pool. Since the recharging is an enzymatic process, we model it using a Michaelis-Menten equation [29]; we assume that the amino acids and other required factors are in plentiful supply and treat the recharging as a single substrate enzymatic process. We take the standard mean-field equations for the TASEP [Eqs. (1)] and introduce an equation to describe the use and recharging of the aa-tRNA pool:

$$\frac{dT}{dt}=\frac{V(\bar{T}-T)}{K_m+\bar{T}-T}-\sum_{i=1}^{L'}k\rho_i(1-\rho_{i+1}), \tag{9}$$

where T is the number of aa-tRNAs and $\bar{T}$ is the total number of tRNAs. $L'=N(L-1)$ gives the total number of sites where tRNAs are used in N mRNAs of length L ($L-1$ since tRNAs are not used at termination sites). The first term in Eq. (9) corresponds to recharging and the second corresponds to the reduction in T every time a particle hops. The parameters V and K_m associated with the recharging are the maximum recharge rate and the number of uncharged tRNAs for which we have half the maximum rate, respectively. As described in [15], we assume that the hopping rate k depends linearly on the number of charged tRNAs,

$$k=rT, \tag{10}$$

where r is some intrinsic translation rate. We expect that k will saturate at some maximum; the linear approximation is justified since we expect that the cell is unlikely to waste resources by overproducing tRNAs.

In considering the steady state of Eq. (9) we identify the term under the sum as the current [Eq. (2)]; using Eq. (10) to eliminate T we find that

$$k=r\bar{T}-\frac{rL'K_mJ}{V-L'J}, \tag{11}$$

i.e., k is itself a function of J. We proceed by employing the "maximum current principle" [30], which states that the maximal current in a TASEP with open boundaries is related to the equivalent system with periodic boundaries,

$$\mathcal{J} = \max[J_{\mathrm{PB}}(\rho)] \quad \text{if} \quad \rho_- > \rho > \rho_+, \tag{12}$$

where J_{PB} is the current in the periodic system. The density ρ_- (ρ_+) is an effective density associated with a reservoir of particles to the left (right) of site $i=1$ ($i=L$) in the open system and is related to the rate $\alpha(\beta)$. Solutions of the periodic system are straightforward: with these boundary conditions the mean density is not a function of position, and Eq. (2) becomes $J_{\mathrm{PB}}=k\rho(1-\rho)$. Using Eq. (11) to eliminate k yields a quadratic in J_{PB}; one of the solutions to this can be disregarded as it gives the unphysical result $J_{\mathrm{PB}}|_{\rho=0} \neq 0$. From the remaining solution we have

$$J_{\mathrm{PB}} = \frac{1}{2}\left\{ \frac{V}{L'} + r\bar{T}\left(1+\frac{K_m}{\bar{T}}\right)\rho(1-\rho) - \sqrt{\left[\frac{V}{L'} + r\bar{T}\left(1+\frac{K_m}{\bar{T}}\right)\rho(1-\rho)\right]^2 - 4\frac{V}{L'}r\bar{T}\rho(1-\rho)} \right\}. \tag{13}$$

In Fig. 2 we show several plots which indicate how $J_{\mathrm{PB}}(\rho)$ depends on the various parameters. From the above equation we identify three important quantities: the maximum internal hopping rate $r\bar{T}$, the ratio of the Michaelis constant and the total number of tRNAs $K_m/\bar{T}$, and the ratio of the maximum recharging rate and the total number of codons where aa-tRNAs can be used V/L', which gives an upper bound for the current J [31]. In the subplots of Fig. 2 we show how each one of these quantities affects $J_{\mathrm{PB}}(\rho)$ while the others are fixed at a value of unity. We note that the shape of the curve ranges from that of the original TASEP $[J=k\rho(1-\rho)]$ to having a flattened top; in particular small values of V/L' and large values of $r\bar{T}$ and $K_m/\bar{T}$ give a function with an apparent plateau. We note however that the curve always remains unimodal with a maximum at $\rho=1/2$.

Throughout this paper, we use parameters which are realistic for the widely studied yeast *S. cerevisiae*. A typical cell contains a total of 3.5×10^6 codons (arranged in mRNAs of typical length $L=500$ codons) and around 3×10^6 tRNAs, and together the number of codons and the number of tRNAs represent the system size. Such large numbers of codons pose a considerable challenge for treatment by simulation, so we rescale the system such that there are $L=500$ codons in each of 100 mRNAs (i.e., $L'=4.99\times10^4$), and $\bar{T}=4.3\times10^4$ tRNAs. This rescaling does not affect intensive quantities such as the current and density, although we note their dependence on L' and $\bar{T}$ separately. The scale of the hopping rate is fixed by the constant r which we take as $r=2.3\times10^{-4}$ s^{-1} so as to give the maximum hopping rate $\bar{k}=r\bar{T}=10$ s^{-1}, which is well established in the literature [1]. The numbers of codons and tRNAs and the mean hopping rate are all well known in the literature, so we use the above rescaled values for the rest of this paper. The parameters for the recharging component of the model are less well known. The maximum recharging rate is given by

$$V = Ek_{\mathrm{cat}},$$

where E is the number of enzymes present in the cell and k_{cat} is the rate at which one enzyme molecule can recharge one tRNA. Each amino acid species has a different associated aminoacylation enzyme, and measured values for k_{cat} and K_m are known for some synthetases [32–36] but not others. For this reason we use values from one typical enzyme—tyrosine tRNA synthetase [37]. The number of enzyme molecules in a typical cell has been measured by von der Haar [38]. Values of K_m are usually quoted as concentrations; since our model has no spatial extent we must multiply this by the cell volume to get a number of tRNAs. We note that to find realistic parameters, both K_m and V (due to its dependence on the number of enzymes) must be scaled with system size, i.e., it is the ratios of E and K_m to $\bar{T}$ which we take from the literature. Hence, for the rescaled values of $\bar{T}$ and L' given above, $V=1.95\times10^3$ s^{-1} and $K_m=497$ tRNAs.

Since the recharging parameters can only be estimated from the literature, we now examine the behavior of the model as these are varied. In Fig. 3 we plot $J_{\mathrm{PB}}(\rho)$ and $J_{\mathrm{PB}}^{\max} \equiv J_{\mathrm{PB}}(1/2)$ at different values of V/L' and K_m. From the plot of maximum current as a function of V/L' with realistic K_m [Fig. 3(a)] we can clearly identify two regimes:

$$\text{case 1:} \quad J_{\mathrm{MC}} \approx \frac{r\bar{T}}{4} \quad \text{for} \quad \frac{V}{L'} > \frac{r(\bar{T}+K_m)}{4},$$

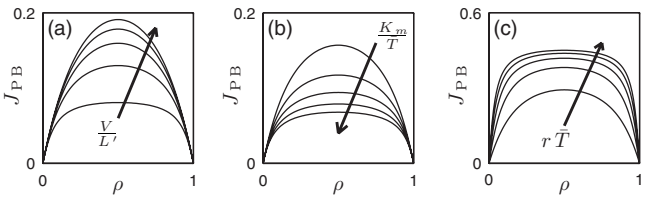

FIG. 2. Plots showing how the values of V/L', $K_m/\bar{T}$, and $r\bar{T}$ affect the shape of the $J_{\mathrm{PB}}(\rho)$ curve. In each case one quantity is varied, and the others are held at unity; the arrow indicates the direction of increasing the varied quantity. In (a) V/L' is varied between 0.2 and 1, in (b) $K_m/\bar{T}$ is varied between 2 and 10, and in (c) $r\bar{T}$ is varied between 2 and 10.

$$\text{case 2:} \quad J_{\mathrm{MC}} \approx \frac{V}{L'}\frac{\bar{T}}{\bar{T}+K_m} \quad \text{for} \quad \frac{V}{L'} < \frac{r(\bar{T}+K_m)}{4}.$$

Large V/L' (case 1) recovers the original TASEP—the recharging process is so fast that effectively all tRNAs are always charged. The maximal current is limited by the steric interactions between the particles. In case 2 (in which lie the above discussed realistic recharging parameters) the maximum current is reduced and increases approximately linearly with V for small values of V. The current density curve [Fig. 3(b)] is severely flattened for case 2 (however, we note that it remains unimodal). From Figs. 3(c) and 3(d) we see that the value of K_m determines the sharpness of the crossover between the two regimes, with the smaller (realistic) value giving the sharper crossover. The physical interpretation of case 2 result is that when there is a small number of particles on the lattice, the recharging machinery can keep up with the aa-tRNA demand and the current increases rapidly with the density, but as the density gets larger the recharging begins to become limiting. The current then increases only very slowly with density, and the maximum current depends on V; we term this regime limited resources (LR). As with other exclusion processes the symmetry about $\rho=1/2$ can be explained by considering the equivalence between particles and holes, which is maintained in this model.

Following the maximal current principle [30], the maximum current in the open boundaries system is equal to that of the periodic system. In the LD phase the current is $\rho=\alpha/k$, and an expression for the current is given by making the replacement $\rho\to\alpha/k$ in the equation for J_{PB}. The hopping rate is now of course itself a function of the current, and

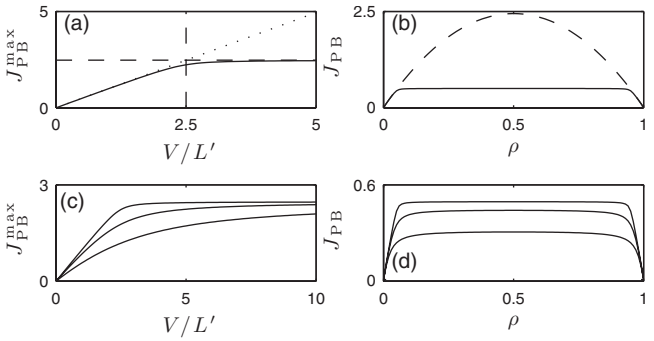

FIG. 3. Plots showing how the recharging parameters affect the current in the periodic system. (a) Plot of the maximal current $\mathcal{J}_{\mathrm{MC}}$ (solid line) as a function of V/L' with $K_m=497$, the realistic value as discussed in the text. The dotted line shows $J=[\bar{T}/(\bar{T}+K_m)](V/L')$, and dashed lines are at $r\bar{T}/4$ (horizontal) and $r(\bar{T}+K_m)/4$ (vertical). (b) Plots showing $J_{\mathrm{PB}}(\rho)$ for $V/L'=10^5$ s^{-1} (case 1—dashed line) and for $V/L'=1.95\times10^3$ s^{-1} (case 2—solid line). In both cases $K_m=497$ tRNAs. (c) Plots showing $\mathcal{J}_{\mathrm{MC}}$ as a function of V/L' at different values of K_m. From top to bottom these are $K_m=497$, 4970, and 24 850 tRNAs. (d) Plots showing $J_{\mathrm{PB}}(\rho)$ for the realistic value for V/L' (see text) at different K_m's, from top to bottom as in (c).

we eliminate k using Eq. (11). The resulting equation has two solutions, again one of which is unphysical ($J\neq0$ for $\alpha=0$). The critical initiation rate where we cross from LD$\to$MC is found when $\rho=\alpha/k=1/2$, i.e., $\alpha^*=k/2$; we again use Eq. (11) to eliminate k and then the expression for $J_{\mathrm{PB}}^{\max}$ to eliminate J. The results can be summarized as follows:

$$\mathcal{J}_{\mathrm{LD}} = \frac{1}{2}\left(\alpha\left[1-\frac{\alpha}{r(\bar{T}+K_m)}\right]+\frac{\bar{T}}{\bar{T}+K_m}\frac{V}{L'}-\sqrt{\left\{\frac{\bar{T}}{\bar{T}+K_m}\frac{V}{L'}+\alpha\left[1-\frac{\alpha}{r(\bar{T}+K_m)}\right]\right\}^2-\frac{4\alpha(r\bar{T}-\alpha)}{r(\bar{T}+K_m)}\frac{V}{L'}}\right)$$

$$\rho_{\mathrm{LD}} = \frac{1}{2\alpha}\left(\alpha\left[1+\frac{\alpha}{r(\bar{T}+K_m)}\right]-\frac{\bar{T}}{\bar{T}+K_m}\frac{V}{L'}+\sqrt{\left\{\frac{\bar{T}}{\bar{T}+K_m}\frac{V}{L'}+\alpha\left[1-\frac{\alpha}{r(\bar{T}+K_m)}\right]\right\}^2-\frac{4\alpha(r\bar{T}-\alpha)}{r(\bar{T}+K_m)}\frac{V}{L'}}\right) \quad \text{for} \quad \begin{matrix}\alpha<\beta\\ \alpha\leq\alpha^*,\end{matrix} \tag{14}$$

$$\mathcal{J}_{\mathrm{MC}} = \frac{1}{2}\alpha^*, \quad \rho_{\mathrm{MC}} = \frac{1}{2}, \quad \text{for} \quad \alpha,\beta\geq\alpha^*, \tag{15}$$

where

$$\alpha^* = \frac{r(\bar{T}+K_m)}{4}+\frac{V}{L'}-\sqrt{\left(\frac{r(\bar{T}+K_m)}{4}+\frac{V}{L'}\right)^2-r\bar{T}\frac{V}{L'}}.$$

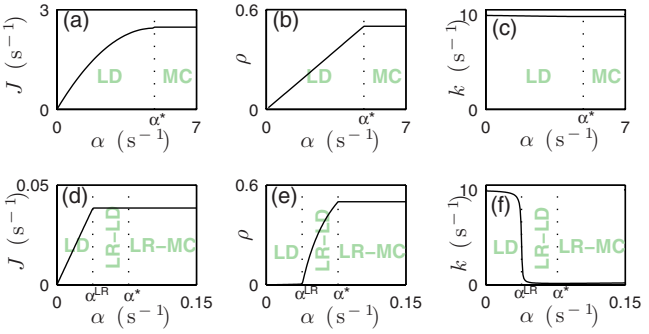

FIG. 4. (Color online) Plots showing mean-field results for the TASEP with finite aa-tRNA recharging but no slow sites. (a)–(c) show J, ρ, and k as functions of α for case 1 ($V/L'=5$; other parameters are given in Sec. III), and (d)–(f) show the same for case 2 (parameters are given in Sec. III). Dotted lines show α_{LD} and α^*. We note that in (e) for $\alpha<\alpha^{\mathrm{LR}}$ the nonzero value of ρ is too small to be seen at this scale.

We do not give equations for the HD phase since, due to hole-particle symmetry, these can be easily obtained from those for LD (e.g., $\mathcal{J}_{\mathrm{HD}}$ is given by the same equation as $\mathcal{J}_{\mathrm{LD}}$, but replacing α with β). For the rest of this paper we do not consider the HD phase and set $\beta \gg k$; since it is thought that translation is not limited by the termination step this is a reasonable assumption for a real cell [39]. For clarity, in this section we use the calligraphic $\mathcal{J}$ to refer to Eqs. (14) and (15) and the standard J with subscripts to denote the approximations in the various regimes. Since $\mathcal{J}_{\mathrm{MC}} \equiv J_{\mathrm{PB}}^{\max}$ cases 1 and 2 as discussed above still apply.

In Figs. 4(a)–4(c) we plot J, ρ, and k as functions of the initiation rate α for case 1 ($V/L'=5$ s^{-1}), and in Figs. 4(d)–4(f) we plot the same for case 2 ($V/L'=0.039$ s^{-1}—the realistic parameters estimated from the literature). In both cases we use the realistic value for K_m from the literature [37]. In case 1 the behavior is as in the original uniform TASEP: J and ρ increase with α until $\alpha=\alpha^*$, where there is a second-order phase transition to the MC phase. In case 2 for small α, J and ρ follow the same profile as in case 1; however, at $\alpha \sim \alpha^{\mathrm{LR}}$ there is a drastic change in the behavior: there appears to be a plateau in J. In actual fact J continues to increase very slowly with α until $\alpha=\alpha^*$, where there is again a phase transition to the MC phase. The reason for the difference in the behavior between cases 1 and 2 is clarified in the plots for k [Figs. 4(c) and 4(f)]: in case 1, k remains constant as the rate at which tRNAs are recharged is always larger than the rate at which they are used; in case 2 for $\alpha>\alpha^{\mathrm{LR}}$ the usage of tRNAs is limited by the recharging rate, so the steady-state charged tRNA abundance T (and therefore k) is reduced. The current cannot increase above $J \approx V/L'$. Thus, for case 2 we have a limited resources regime within the low-density phase (LR-LD), and the maximal current is reduced (LR-MC).

In summary, for case 1 $[V/L'>r(\bar{T}+K_m)/4]$ we regain the results from the original TASEP:

$$J_{\mathrm{LD}} \approx \alpha\left(1-\frac{\alpha}{r\bar{T}}\right), \quad \rho_{\mathrm{LD}} \approx \frac{\alpha}{r\bar{T}}, \quad \text{for } \alpha<\beta, \alpha \le \alpha^*,$$

$$J_{\mathrm{MC}} \approx \frac{r\bar{T}}{4}, \quad \rho_{\mathrm{MC}} \approx \frac{1}{2}, \quad \text{for } \alpha,\beta \ge \alpha^*,$$

$$\alpha^* \approx \frac{r\bar{T}}{2}, \tag{16}$$

by expanding Eqs. (14) about $\alpha=0$ to second order and taking the limit $V\to\infty$ in Eq. (15). As α is increased we observe the transition LD$\to$MC.

For case 2 $[V/L'<r(\bar{T}+K_m)/4]$, which is the biologically relevant parameter regime, it is possible to estimate the current and density in LD by expanding Eqs. (14) about $V=0$ to first order. The current in the LR-MC regime can be approximated by expanding Eq. (15) about $V=0$ to first order. If K_m is small (as in the realistic parameters) we can approximate that the current in the LR-LD regime is equal to that in LR-MC. More precisely, small K_m gives a sharp crossover between cases 1 and 2 [Fig. 3(c)] and a sharp well-defined crossover between LD and LR-LD at α^{LR} [Fig. 3(d)]. We find

$$J_{\mathrm{LD}} \approx \alpha\left(1-\frac{\alpha}{r\bar{T}}\right), \quad \rho_{\mathrm{LD}} \approx \frac{\alpha}{r\bar{T}}, \quad \text{for } \alpha<\beta, \alpha \le \alpha^{\mathrm{LR}},$$

$$J_{\text{LR-LD}} \approx \frac{\bar{T}}{\bar{T}+K_m}\frac{V}{L'}, \quad \text{for } \alpha^{\mathrm{LR}} \le \alpha^*,$$

$$J_{\text{LR-MC}} \approx \frac{\bar{T}}{\bar{T}+K_m}\frac{V}{L'}, \quad \rho_{\text{LR-MC}} \approx \frac{1}{2}, \quad \text{for } \alpha,\beta \ge \alpha^*,$$

$$\alpha^{\mathrm{LR}} \approx \frac{\bar{T}}{\bar{T}+K_m}\frac{V}{L'}, \quad \alpha^* \approx 2\frac{\bar{T}}{\bar{T}+K_m}\frac{V}{L'}. \tag{17}$$

The estimate for α^{LR} is found by equating J_{LD} and $J_{\text{LR-MC}}$, solving for α, and again only keeping terms up to first order in V. As α is increased we observe the transitions LD$\rightsquigarrow$LR-LD$\to$LR-MC. The curly arrow indicates that there is no phase transition between LD and LR-LD: the crossover between LD and LR-LD is always smooth (there are no discontinuities in higher derivatives with respect to α), and α^{LR} is only well defined for small K_m.

Crucially, the realistic parameters discussed above fall well within case 2 $[V/L' \approx 0.039$ s^{-1} and $r(\bar{T}+K_m)/4 \approx 2.5$ s$^{-1}]$. Although the recharging parameters are not known for all tRNA species, those which are available fall so far within case 2 that we expect no qualitative difference in the results with respect to small changes; we therefore use these values throughout the rest of the paper.

III. TASEP WITH FINITE RECHARGING AND A SLOW SITE

In this section we extend our model with finite recharging of aa-tRNA to include slow codons. As we have seen, even with only a single tRNA species, finite recharging has a ma-

jor impact on the dynamics of a system where the parameters fall into case 2 (the biologically realistic regime, as shown above). If there are multiple types of codons one would expect competition effects to be even more important. Since it is analytically tractable, we consider the simple designer mRNA with a single central defect codon.

We study a TASEP where codons have a hopping rate $k_i=k$ for $i\neq L/2$ and $k_{L/2}=q$ and allow k and q to vary with the number of aa-tRNAs,

$$k = rT_k, \quad q = rT_q, \tag{18}$$

where T_k and T_q are the numbers of charged aa-tRNAs of each species and r is an intrinsic hopping rate as before. Similarly to Sec. II B, we define the ratio

$$s = \frac{\bar{T}_q}{\bar{T}_k}, \tag{19}$$

as a measure of the intrinsic speed of the slow site relative to the other sites, where $\bar{T}_q$ and $\bar{T}_k$ are the total numbers of tRNAs of each type. We examine the behavior of the system as a function of both s and the initiation rate α. Again the recharging is modeled using a Michaelis-Menten equation, and the rates at which tRNAs are recharged are

$$V_k\frac{\bar{T}_k - T_k}{K_k + \bar{T}_k - T_k}, \quad V_q\frac{\bar{T}_q - T_q}{K_q + \bar{T}_q - T_q},$$

for types k and q, respectively. As detailed in the previous section, in general different tRNAs are recharged by different enzymes, but for simplicity we assume $K_k=K_q=K_m$. As in Sec. II C we again preserve the ratio of the number of enzymes to the number of the relevant tRNA molecules found experimentally, and now we assume that this is the same for all tRNA types and that the different enzymes have the same k_{cat} values [32–36]. We therefore fix V_k based on the value of $\bar{T}_k$ and set $V_q=sV_k$. These choices are reasonable since many of the known parameters for synthetases have similar values. We keep the same parameter values for the k-type tRNAs as in Sec. II C, defining $\bar{T}_k=4.3\times10^4$ and $V_k=1.95\times10^3$ s^{-1}. The total number of k-type codons is $L''=N(L-2)$ since there is one q-type codon and one termination codon per mRNA.

We now derive a mean-field model by combining the approaches described in Secs. II B and II C [15,27]. The use and recharging of the tRNAs are now described by

$$\frac{dT_k}{dt} = \frac{V_k(\bar{T}_k - T_k)}{K_m + \bar{T}_k - T_k} - \sum_{i\neq L/2,L} k\rho_i(1-\rho_{i+1}), \tag{20}$$

$$\frac{dT_q}{dt} = \frac{sV_k(\bar{T}_q - T_q)}{K_m + \bar{T}_q - T_q} - Nq\rho_{L/2}(1-\rho_{L/2+1}), \tag{21}$$

where the sum in Eq. (20) is over k-type codons on all mRNAs. By following the same procedure as in Sec. II C we find that in the steady state we have the following hopping rates:

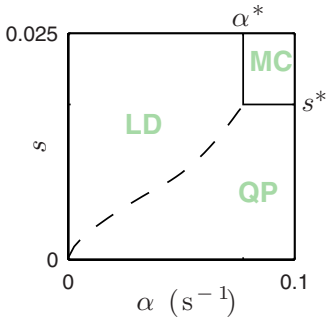

FIG. 5. (Color online) Plot showing the phase plane in α and s. The dashed line shows the first-order transition QP→LD at α^{QP}, and the solid lines show the continuous phase transition to the MC phase at α^* (vertical) and s^* (horizontal), all found from the mean-field analysis (see the Appendix). The LR regimes within the QP and LD phases are not shown. Parameters are given in the text.

$$k(J) = r\bar{T}_k - \frac{rL''K_mJ}{V_k - L''J}, \tag{22}$$

$$q(J) = rs\bar{T}_k - \frac{rNK_mJ}{sV_k - NJ}, \tag{23}$$

i.e., k and q are both functions of J. We identify the current (which must be constant throughout the lattice) as

$$J = k\rho_i(1-\rho_{i+1}) = q\rho_{L/2}(1-\rho_{L/2+1}). \tag{24}$$

Assuming that we can treat the system as two sublattices connected across the slow site, we define α_{eff} and β_{eff} as in Eq. (4), leading to the current

$$J = \frac{\alpha_{\text{eff}}\beta_{\text{eff}}}{q(J)},$$

which differs from the original TASEP with a slow site in that q is itself a function of J.

We show a full treatment of the mean-field model in the Appendix and present only the results here. As in the work of Kolomeisky [27] there exist LD and HD phases, an MC phase, and a QP phase; we assume $\beta\gg\alpha,\bar{k}$ and concentrate on the phase diagram in the α-s plane (Fig. 5). From the mean-field model we find transitions to MC at α^* and s^*, and the QP-LD phase boundary at $\alpha^{\text{QP}}=f(s)$. In contrast to the original TASEP with a slow site, the latter boundary is a function of s.

As with the uniform lattice, for case 2 parameters we see a LR regime within the LD phase and a dramatic reduction in the maximal current [Eqs. (17)]. The major result of this paper is that we also now see an LR regime within the QP phase.

In Figs. 6(a)–6(d) we show color plots of J, ρ, $\Delta\rho=\rho_l-\rho_r$, and k as functions of both α and s for case 2 parameters (since they are biologically realistic). We show both mean-field and Monte Carlo simulation results, the discussion of the latter we postpone until Sec. III B. We can clearly identify several regimes:

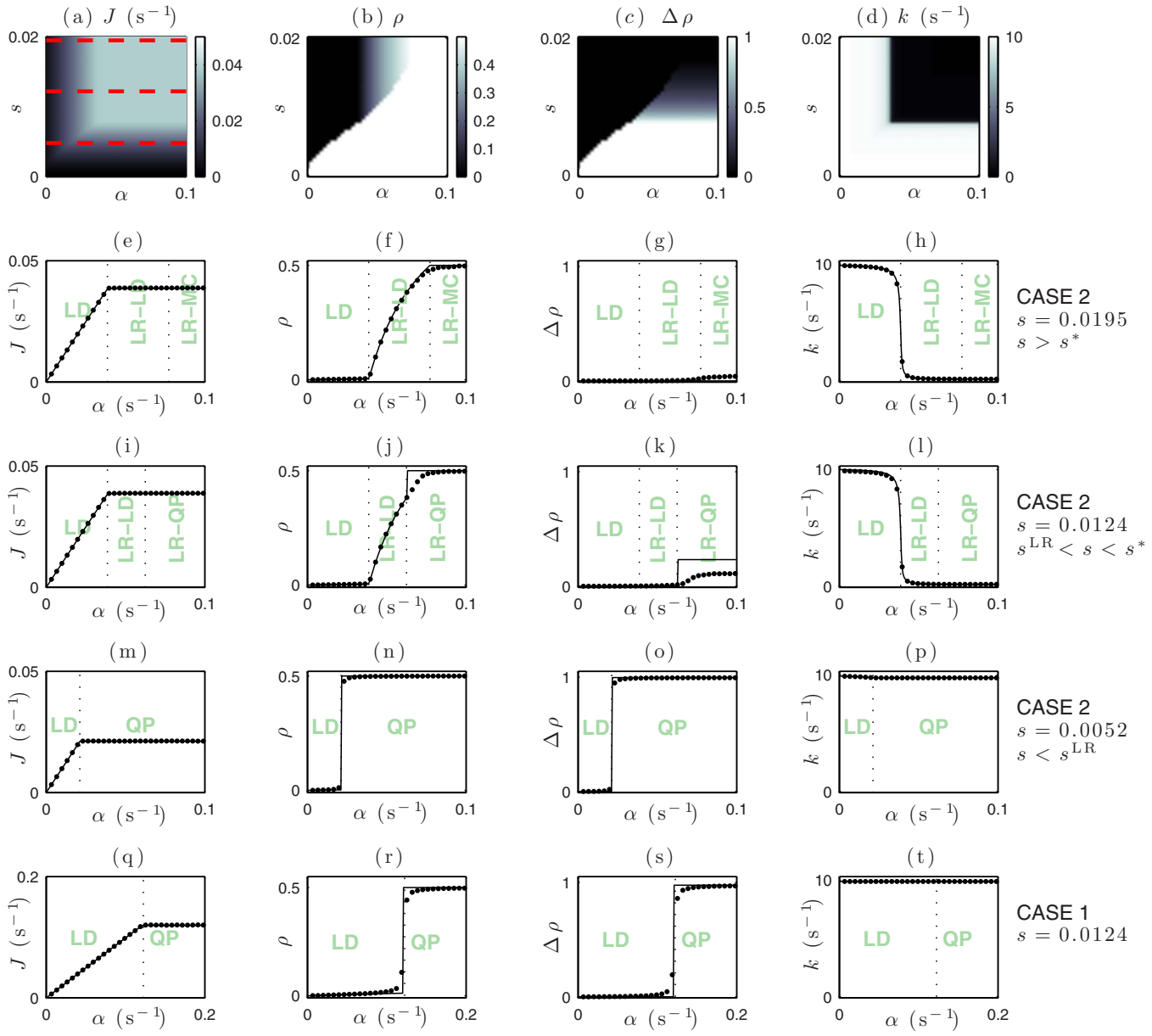

FIG. 6. (Color online) (a)–(d) Color plots showing mean-field results for J, ρ, $\Delta\rho$, and k for the biologically realistic (case 2) parameters given in the text. Plots (e)–(h), (i)–(l), and (m)–(p) show the same results for J, ρ, $\Delta\rho$, and k as functions of α at constant s, with $s>s^*$, $s^{LR}<s<s^*$, and $s<s^{LR}$, respectively. For comparison, plots (q)–(t) show the $s^{LR}<s<s^*$ results but for case 1 parameters ($V_k=10^6$ s^{-1} and other parameters unchanged), where the behavior of the original TASEP is recovered. Lines show the mean-field model and points show the MCS results. The red dashed lines in (a) indicate the values of s in (e)–(t).

LD: As in the original TASEP model, there is a low density and $J \propto \alpha$. The hopping rate is approximately constant $k \approx r\bar{T}_k$.

LR-LD: As in the uniform TASEP with finite recharging, J is approximately constant and k is reduced.

LR-MC: Again as in the uniform TASEP with finite recharging, k is reduced and J constant with respect to both α and s, but has a value much smaller than the maximal current seen for case 1 parameters.

QP: Similar to the original TASEP with a slow site, J is independent of α, but is proportional to s; $\Delta\rho \approx (1-s)/(1+s)$ indicates a queue, and the hopping rate is approximately constant $k \approx r\bar{T}_k$.

LR-QP: This is another LR regime within the QP which is not present in other models. There is still queuing, as indicated by nonzero $\Delta\rho$; however, $\Delta\rho \ll (1-s)/(1+s)$, and this is accompanied by a reduced hopping rate $k \ll r\bar{T}_k$, indicating limited resource availability. We denote the value of s at which we move to the LR-QP regime s^{LR} and discuss this in Sec. III A.

In Figs. 6(e)–6(p) we show three cross sections at constant s [indicated in Fig. 6(a)]. Here, we see more clearly the different phases and regimes and compare with the MCS results (discussion of which we postpone until Sec. III B). For comparison, in Figs. 6(q)–6(t) we show mean-field results for case 1 parameters, which are the same as for the

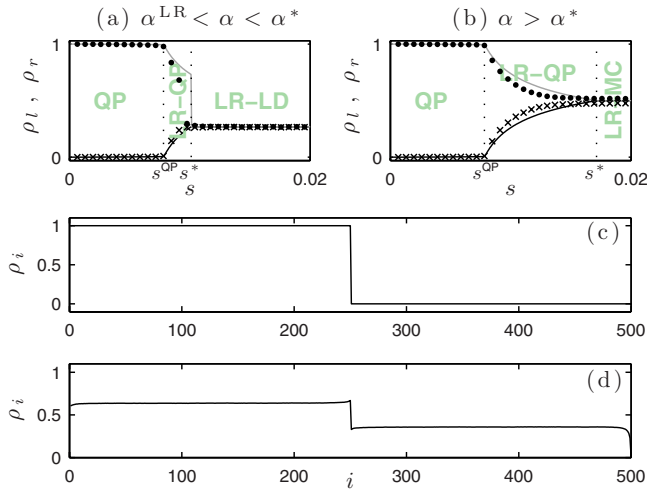

FIG. 7. (Color online) Top: plots showing ρ_l and ρ_r as functions of s (black and gray lines, respectively) for (a) α=0.0528 s^{-1} ($\alpha^{LR}<\alpha<\alpha^*$) and (b) α=0.099 s^{-1} ($\alpha>\alpha^*$). Points show MCS results. The location of the phase transition to the QP can be found by considering the inverse of the function for α^{QP}, i.e., $s^{QP}=f^{-1}(\alpha^{QP})$ (see text). Middle and bottom: plots showing density as a function of codon position for (c) α=0.099 s^{-1}, $s=7\times10^{-4}$ (pure QP) and (d) α=0.099 s^{-1}, s=0.01 (mixed LR-QP). Other parameters are in the text.

original TASEP with a slow site: as α increases the current continues to increase until $\alpha=\alpha^{QP}$, and $\Delta\rho=(1-s)/(1+s)$ throughout the QP. For $s>s^*$ [Figs. 6(e)–6(h)] the transition LD$\rightsquigarrow$LR-LD occurs at α^{LR}, and there is a continuous phase transition LR-LD$\rightarrow$LR-MC at α^*, just as in the system without a defect site. For case 2 with $s^{LR}<s<s^*$ [Figs. 6(i)–6(l)] as α is increased, again the transition LD$\rightsquigarrow$LR-LD occurs at α^{LR}, but as α increases further there is a first-order phase transition LR-LD$\rightarrow$LR-QP. For $s<s^{LR}$ the system does not enter a limited resources phase, and as α is increased there is a first-order phase transition LD$\rightarrow$QP as would be seen in the original TASEP with a slow site.

We now consider in more detail the LR-QP regime. In Figs. 7(a) and 7(b) we show how ρ_l and ρ_r vary with s for two different values of α. In the LR-QP regime due to limited resources the severity of the queuing has decreased; the difference between this mixed queuing with limited resources behavior and that of the pure QP is shown in density plots in Figs. 7(c) and 7(d). In the pure QP, particles enter the rightmost half of the lattice only very rarely (α_{eff} is small), and then move quickly through the lattice before leaving, resulting in a very low density. In the LR-QP regime the hopping rate k is reduced, so particles which enter the rightmost sublattice move more slowly, taking a longer time to reach the end of the lattice; the result is that the density is larger than in the pure QP. We can treat the leftmost sublattice as having a low density of holes which enter at the right and hop leftward with rate k; in the LR-QP regime, holes spend more time on the lattice, so the hole density is larger, i.e., ρ_l is lower, than in the pure QP. We emphasize that the LR-QP regime does not exist in the original TASEP, to which our present model reduces for biologically unrealistic case 1 parameters.

A. Estimation of α^{LR} and s^{LR}

The initiation rate α^{LR} and extrinsic speed s^{LR} represent the values of α and s where the rate at which k-type aa-tRNAs are being used approaches the rate at which they can be recharged. These quantities are not well defined since, as discussed above, there is not a true phase transition. The sharpness of the crossover between LD$\rightsquigarrow$LR-LD and QP$\rightsquigarrow$LR-QP depends on the value of K_m, so α^{LR} and s^{LR} cannot be found exactly from the mean-field model. However, for the realistic parameters we use here, K_m is small so the crossover is sharp, and it is possible to estimate α^{LR} as was done for the uniform TASEP [Eqs. (17)]. In this section we show that this approximation is consistent with heuristic physical reasoning, and then use this same reasoning to find an expression for s^{LR}.

As in Sec. II C, an estimate of α^{LR} can be found by expanding the equation for $\mathcal{J}_{LD}$ about $V_k=0$ and equating this with the expansion of $\mathcal{J}_{MC}$ about $V_k=0$. Keeping terms to first order gives $\alpha^{LR}\approx(V_k/L'')\bar{T}_k/(\bar{T}_k+K_m)$. The same expression can be found by considering the rate of use ϕ and recharging ψ of tRNAs in the LD phase. The rate at which k-type aa-tRNAs are used in LD is given by $J_{LD}L''$ since the current is defined as the rate at which particles hop out of each site. Since we know the approximation for J_{LD} from Eqs. (17) (which is also valid for the model with a slow site) the rate of k-type aa-tRNA use is approximately,

$$\phi_k=\alpha\left(1-\frac{\alpha}{r\bar{T}_k}\right)L''. \tag{25}$$

The maximum rate at which k-type tRNAs are recharged is realized when $T_k=0$ and is given by

$$\psi_k=\frac{V_k\bar{T}_k}{\bar{T}_k+K_m}. \tag{26}$$

Equating ϕ_l and ψ_k gives the critical value of α; we are left with a quadratic in α^{LR}, again with one solution which can be disregarded as unphysical since it gives $\alpha^{LR}\neq0$ for $V_k=0$. The remaining solution gives

$$\alpha^{LR}=\frac{r\bar{T}_k}{2}\left(1-\sqrt{1-4\frac{V_k}{L''}\frac{\bar{T}_k}{\bar{T}_k+K_m}\frac{1}{r\bar{T}_k}}\right), \tag{27}$$

which, when only keeping terms to first order in V_k, gives $\alpha^{LR}\approx(V_k/L'')\bar{T}_k/(\bar{T}_k+K_m)$—the same result as the estimate from the mean-field theory.

An expression for s^{LR} can be found via similar arguments. We now consider starting in the QP phase; again the rate of aa-tRNA use is JL''. In the rightmost half of the lattice there is a low density of particles, and we can approximate the current $J_{LD}\approx\alpha_{\text{eff}}(1-\alpha_{\text{eff}}/r\bar{T}_k)$. From Eq. (4) we have by definition $\alpha_{\text{eff}}=\rho_{L/2}q$, where $\rho_{L/2}$ is the density at the slow site. Since for the parameter range studied here we never reach a regime were q-type aa-tRNAs become depleted, we can approximate $q\approx rs\bar{T}_k$, so the rate of k-type aa-tRNA use in QP is

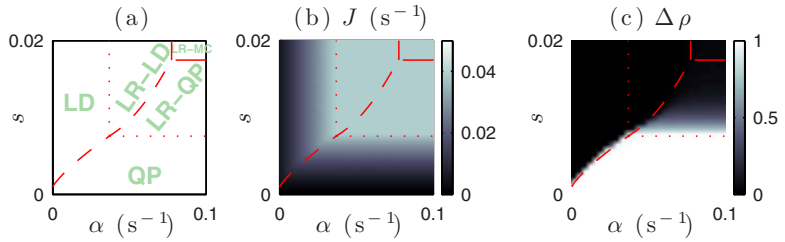

FIG. 8. (Color online) (a) Phase plane plot from mean-field treatment showing the different regimes and phases for biologically realistic case 2 parameters. Solid lines show continuous phase transitions at α^* and s^* and the dashed line shows the first-order transitions at α^{QP}; dotted lines show α^{LR} and s^{LR}, bounding the region where the current becomes limited by the finite recharging of the aa-tRNAs. Plots (b) and (c) show MCS results with lines showing the transitions as in (a).

$$\psi_k = L''\rho_{L/2} r s \bar{T}_k (1 - \rho_{L/2} s). \tag{28}$$

Although in the bulk of the leftmost sublattice we can approximate that the density is given by ρ_l, due to spatial correlations in the density around the slow site our mean-field model cannot predict the value of $\rho_{L/2}$. Instead, since far to the left of this site $\rho_{\mathrm{bulk}} \approx 1$ and far to the right $\rho_{\mathrm{bulk}} \approx 0$, we assume that $\rho_{L/2} \approx 1/2$. If we consider increasing s then we would expect to move to the LR regime when the quantities in Eqs. (26) and (28) are equal, i.e., at

$$s^{\mathrm{LR}} = 1 - \sqrt{1 - 4\frac{V_k}{L''}\frac{1}{r(\bar{T}_k + K_m)}}, \tag{29}$$

which is independent of α. Keeping only terms to first order in V_k gives

$$s^{\mathrm{LR}} \approx \frac{V_k}{L''}\frac{2}{r(\bar{T}_k + K_m)}.$$

Although we do not have an analytical expression for the current in the QP (see the Appendix), we are still able to estimate the value of s^{LR}. This approximation agrees well with the MCS discussed below.

B. Monte Carlo simulation results

We test our mean-field prediction by comparing with Monte Carlo simulations. These proceed via a similar scheme to those in previous studies; we use continuous time Monte Carlo [40] as this is very efficient. Particles which are to the left of a vacant site are picked stochastically such that they move with a rate k_i. Initiation is allowed for by a zeroth site associated with each lattice that always contains a particle, which enters the lattice with rate α provided there is a vacancy. In the present model we choose not only from the $N(L+1)$ sites, but also from any of the $\bar{T}_k + \bar{T}_q$ tRNAs which are uncharged, such that recharging occurs with a rate $V_k/(K_m + \bar{T}_k - T_k)$ or $sV_k/(K_m + \bar{T}_q - T_q)$ depending on the tRNA type. Every time a particle hops or a tRNA is recharged, we update T_k and T_q accordingly. To remove any transient effects associated with the initial conditions we disregard the first 6×10^3 s of each simulation and run for a further 6×10^3 s.

Despite the fact that the mean-field treatment ignores the significant spatial correlations induced near the slow site, the solutions for J, ρ, and k fit well to the simulation results. Our mean-field model fares less well in predicting the bulk densities to the left and right of the slow site (ρ_l, ρ_r, and therefore $\Delta\rho$) in the LR-QP regime [Figs. 6(k) and 7]. This is due to the significant spatial correlations in the density induced near the slow site. It is not surprising that correlations increase in the LR regime, as here the different lattices are coupled via the tRNA population. Nevertheless, we have been able to accurately predict the existence of the LR regime within the QP. Figure 8 shows color plots for J and $\Delta\rho$ from the simulation results, together with the phase boundaries at α^* and s^*, and the boundaries for the LR-LD and LR-QP regimes at α^{LR} and s^{LR} from the mean-field treatment.

IV. DISCUSSION AND CONCLUSIONS

We have examined the effect of slow codons in a TASEP model of mRNA translation which includes finite recharging of aa-tRNA molecules. As discussed in [15], including finite aa-tRNA recharging in a uniform mRNA leads to substantially different behavior compared to the original TASEP. For biologically realistic parameters (case 2), there is a regime where limited resource availability prevents the current from increasing above a maximum value which is much lower than the maximal current in the original TASEP. This regime is characterized by a severe reduction in the charging rate of aa-tRNAs. We have LR for $\alpha > \alpha^{\mathrm{LR}}$, because the rate at which aa-tRNAs are used cannot increase above the rate at which they are recharged. For the biologically relevant case of $K_m \ll \bar{T}$, α^{LR} is approximately independent of the total abundance of aa-tRNAs, $\bar{T}$, and other parameters such as the intrinsic translation rate r. Although this robustness to changes in r and $\bar{T}$ is a result of our choice that the hopping rate k depends linearly on $\bar{T}$, this is a justified approximation as we expect the value of $\bar{T}$ to be below any saturation point—the cell is unlikely to overproduce tRNAs on energetic grounds. The sharp reduction in aa-tRNA charging levels in the LR phase is a hallmark of this effect [compare Figs. 4(c) and 4(f)]. This has not been present in previous models, and since it is such a large effect, it will be easily observable experimentally.

We have shown that a queuing phase exists in a model with finite recharging for an mRNA with a single slow codon

in the center. We follow the method of Kolomeisky [27], and although this simple mean-field approach does not take into account any correlations induced by the slow site, we are nevertheless able to predict the existence of a limited resources regime. The main result of this model is the existence of a limited resources regime *within* the queuing phase. We are able to predict with reasonable accuracy the current in the different regimes, as well as the locations of the phase transitions. Qualitative arguments have also allowed us to find analytical expressions for the critical initiation rate α^{LR} and critical speed of the slow codon s^{LR} beyond which the system enters the LR regime. In the LR regime within the QP, we see a reduction in the severity of queuing; although due to spatial correlations in the density our mean-field model fails to accurately predict the difference in density either side of the slow site, the behavior is qualitatively the same as in the Monte Carlo simulations. The coupling between the lattices (and between particles on the same lattice) via the tRNA pool leads to increased correlations: we note that, for example, Eqs. (20) and (21) become highly susceptible to fluctuations at small k (i.e., in LR), and large fluctuations in k will affect all particles simultaneously.

Other authors have made attempts at including the effect of spatial correlations [13,26]. Since we focus on the steady state of the system, where $k(J)$ and $q(J)$ are constant in time, it may be possible to incorporate finite recharging into numerical models such as the finite segment mean-field model of Chou and Lakatos [13]. Their method involves the numerical computation of the eigenvectors of a transition matrix for several sites around the slow site. One could attempt an iterative approach using an estimate of J to give initial values of $k(J)$ and $q(J)$; these would be used to find an improved estimate of J leading to new $k(J)$ and $q(J)$, and so on. The aim of the present work was to gain understanding of the different phase transitions rather than calculate precise values for this anyway rather contrived mRNA, so the mean-field approach was more appropriate.

Other improvements to the model include considering the fact that ribosomes actually cover several codons around the one that is being translated. Several authors have included extended particles in TASEP models [23,24,26,41,42]; incorporation of this in the present model via the approach of Lakatos and Chou [41] is straightforward, although we expect the induced spatial correlations in the density not accounted for by the mean-field approach to become more significant. Also, recently Ciandrini *et al.* [43] included in a TASEP model the fact that a ribosome actually has multiple internal states; a similar approach could be incorporated here by treating the binding of the aa-tRNA to the ribosome and the translocation of the ribosome to the next codon site separately.

The next step in the development of this model will be to examine realistic mRNA sequences with all 41 tRNA and codon types represented. Although some authors [26] have attempted to study real mRNAs using an iterative approach, it is likely that an analytical treatment of such complicated sequences will not be possible, and Monte Carlo simulations will be the only viable option. In the present work we have encountered a regime where the availability of the majority tRNA becomes limited; in a system with 41 tRNA types, it is also likely that minority tRNA type will become limited, and that the related codons become slow and cause queuing. The balance between the supply and the demand is likely to be even more crucial in this case.

In summary, in a TASEP with a slow site, a finite rate of aa-tRNA recharging leads to a limited resources regime within both the low-density and queuing phases. Within the latter, limited resources lead to a reduction in the severity of the queuing.

ACKNOWLEDGMENTS

The authors thank C. Grebogi, I. Stansfield, L. Ciandrini, and S. Heldt for helpful discussions, and BBSRC (Contracts No. BB/F00513/X1 and No. BB/G010722) and RCUK for funding.

APPENDIX

Here, we derive the mean-field results as presented in Figs. 4 and 5. We follow the reasoning of Kolomeisky [27] and assume that each half of the lattice can exist independently in each of the three phases of the original TASEP; as explained in Sec. II A there are four possibilities: LD/LD, HD/HD, MC/MC, and HD/LD, which we also denote QP. Which phase each sublattice is in depends on the effective entry and exit rates as defined in Eq. (4), and the current is given by

$$J = \frac{\alpha_{\mathrm{eff}}\beta_{\mathrm{eff}}}{q(J)}. \tag{A1}$$

We assume that when each sublattice is in the same phase the behavior is the same as for the uniform lattice, so the expressions for current and density follow as in Sec. II C,

$$\mathcal{J}_{\mathrm{LD}} = \frac{1}{2}\left(\alpha\left[1-\frac{\alpha}{r(\bar{T}_k+K_m)}\right]+\frac{\bar{T}_k}{\bar{T}_k+K_m}\frac{V_k}{L''}-\sqrt{\left\{\frac{\bar{T}_k}{\bar{T}_k+K_m}\frac{V_k}{L''}+\alpha\left[1-\frac{\alpha}{r(\bar{T}_k+K_m)}\right]\right\}^2-\frac{4\alpha(r\bar{T}_k-\alpha)}{r(\bar{T}_k+K_m)}\frac{V_k}{L''}}\right),$$

$$\rho_{\mathrm{LD}} = \frac{1}{2\alpha}\left(\alpha\left[1+\frac{\alpha}{r(\bar{T}_k+K_m)}\right]-\frac{\bar{T}_k}{\bar{T}_k+K_m}\frac{V_k}{L'}+\sqrt{\left\{\frac{\bar{T}_k}{\bar{T}_k+K_m}\frac{V_k}{L'}+\alpha\left[1-\frac{\alpha}{r(\bar{T}_k+K_m)}\right]\right\}^2-\frac{4\alpha(r\bar{T}_k-\alpha)}{r(\bar{T}_k+K_m)}\frac{V_k}{L'}}\right), \tag{A2}$$

$$\mathcal{J}_{\mathrm{MC}} = \frac{1}{2}\alpha^*, \quad \rho_{\mathrm{MC}} = \frac{1}{2}, \tag{A3}$$

where

$$\alpha^* = \frac{r}{4}(\bar{T}_k + K_m) + \frac{V_k}{L''} - \sqrt{\left(\frac{r}{4}(\bar{T}_k + K_m) + \frac{V_k}{L''}\right)^2 - r\bar{T}_k\frac{V_k}{L''}}. \tag{A4}$$

As with the uniform lattice, for our realistic (case 2) parameters we see an LR regime within the LD phase and a dramatic reduction in the maximal current. The approximations in Eqs. (16) and (17) still hold.

Since we now have two sublattices, in order to find conditions on α and β which determine whether the system is in the LD or MC phase, we must also consider α_{eff} and β_{eff}. Analogously to Sec. II B, for both sublattices to be in LD we require

$$\mathrm{LD}: \alpha < \beta_{\mathrm{eff}}, \quad \alpha_{\mathrm{eff}} < \beta, \quad \alpha \le \alpha^*, \quad \alpha_{\mathrm{eff}} \le \alpha^*.$$

By equating the LD current in the leftmost sublattice [Eqs. (A2)] with the LD current for the rightmost sublattice (the same equation but with the replacement $\alpha \to \alpha_{\mathrm{eff}}$), we find $\alpha_{\mathrm{eff}} = \alpha$; using Eq. (A1) gives $\beta_{\mathrm{eff}} = q\mathcal{J}_{\mathrm{LD}}/\alpha$, leading to the inequalities

$$\mathrm{LD}: \alpha < \beta, \quad \alpha \le \alpha^*, \quad \alpha^2 < q\mathcal{J}_{\mathrm{LD}}. \tag{A5}$$

We remind the reader that $\mathcal{J}_{\mathrm{LD}}$ is itself a function of α, and note that it is not possible to algebraically isolate α in the latter of inequalities (A5) in order to define the phase boundary $\alpha^{\mathrm{QP}} = f(s)$. Instead we eliminate q using Eq. (23) and isolate s to find

$$s^{\mathrm{QP}} = g(\alpha) = \frac{1}{2}\left[\frac{\mathcal{J}_{\mathrm{LD}}^2 r\bar{T}_k + \frac{V_k}{N}\alpha^2}{\mathcal{J}_{\mathrm{LD}} r\bar{T}_k \frac{V_k}{N}} - \sqrt{\left(\frac{\mathcal{J}_{\mathrm{LD}}^2 r\bar{T}_k + \frac{V_k}{N}\alpha^2}{\mathcal{J}_{\mathrm{LD}} r\bar{T}_k \frac{V_k}{N}}\right)^2 + 4\frac{\mathcal{J}_{\mathrm{LD}} K_m}{V_k/N}}\right],$$

where we note again that $\mathcal{J}_{\mathrm{LD}}$ is itself a function of α. The value of α^{QP} is then given by the inverse of this function, $f(s) = g^{-1}(s)$. Hence, the third inequality of Eq. (A5) is equivalent to $\alpha < f(s)$.

If the system is in the MC phase, we require

$$\mathrm{MC}: \alpha, \beta > \alpha^*, \quad \alpha_{\mathrm{eff}}, \beta_{\mathrm{eff}} > \alpha^*,$$

with the latter implying $\alpha_{\mathrm{eff}}\beta_{\mathrm{eff}} > \alpha^{*2}$; using Eq. (A1) gives

$$\mathrm{MC}: \alpha > \alpha^*, \quad \beta > \alpha^*, \quad \mathcal{J}_{\mathrm{MC}} q > \alpha^{*2}. \tag{A6}$$

The third inequality is independent of α and gives s^*, so that we are in MC if $s > s^*$. Using Eqs. (A5) and (A6) allows us to plot the phase plane (Fig. 5) in terms of α and s.

In the QP we find, by equating the current in each sublattice and disregarding the unphysical solution, that $\alpha_{\mathrm{eff}} = \beta_{\mathrm{eff}}$. To find the current we consider that the rightmost sublattice is in the LD phase, so we can use $\mathcal{J}_{\mathrm{LD}}$ from Eq. (A2), but with the replacement $\alpha \to \alpha_{\mathrm{eff}}$. Eliminating α_{eff} and q using Eqs. (A1) and (23) yields a sixth-order polynomial in $\mathcal{J}_{\mathrm{QP}}$,

$$0 = A_1\mathcal{J}_{\mathrm{QP}} + A_2\mathcal{J}_{\mathrm{QP}}^2 + A_3\mathcal{J}_{\mathrm{QP}}^3 + A_4\mathcal{J}_{\mathrm{QP}}^4 + A_5\mathcal{J}_{\mathrm{QP}}^5 + A_6\mathcal{J}_{\mathrm{QP}}^6, \tag{A7}$$

where the coefficients A_{1-6} are functions of the fixed parameters and s. This cannot be solved analytically, so for the plots we find $\mathcal{J}_{\mathrm{QP}}$ numerically [44,45]. We estimate the density in the QP as in Sec. II B by approximating that this is constant in each half of the lattice. Since the rightmost half of the lattice is in LD, ρ_r is given by the equation for ρ_{LD} in Eqs. (A2) with the replacement $\alpha \to \alpha_{\mathrm{eff}} = \sqrt{\mathcal{J}_{\mathrm{QP}} q(\mathcal{J}_{\mathrm{QP}})}$, and $\rho_l = 1 - \rho_r$. We then find numerical solutions for ρ_l and ρ_r using our solution for $\mathcal{J}_{\mathrm{QP}}$.

[1] B. Alberts, A. Johnson, P. Walter, and J. Lewis, *Molecular Biology of the Cell*, 5th ed. (Garland Publishing Inc., New York, 2008).

[2] V. Popkov, L. Santen, A. Schadschneider, and G. M. Schütz, J. Phys. A **34**, L45 (2001).

[3] P. Pierobon, in *Traffic and Granular Flow '07*, edited by C. Appert-Rolland, F. Chevoir, P. Gondret, S. Lassarre, J.-P. Lebacque, and M. Schreckenberg (Springer, Berlin, 2009), p. 679.

[4] C. T. MacDonald, J. H. Gibbs, and A. C. Pipkin, Biopolymers **6**, 1 (1968).

[5] B. Derrida, E. Domany, and D. Mukamel, J. Stat. Phys. **69**, 667 (1992).

[6] G. Schütz and E. Domany, J. Stat. Phys. **72**, 277 (1993).

[7] R. J. Harris and R. B. Stinchcombe, Phys. Rev. E **70**, 016108 (2004).

[8] M. Robinson, R. Lilley, S. Little, J. Emtage, G. Yarranton, P. Stephens, A. Millican, M. Eaton, and G. Humphreys, Nucleic Acids Res. **12**, 6663 (1984).

[9] M. A. Sørensen, C. G. Kurland, and S. Pedersen, J. Mol. Biol. **207**, 365 (1989).

[10] R. Brockmann, A. Beyer, J. J. Heinisch, and T. Wilhelm, PLOS Comput. Biol. **3**, e57 (2007).

[11] I. J. Purvis, A. J. E. Bettany, T. C. Santiago, J. R. Coggins, K.

Duncan, R. Eason, and A. J. P. Brown, J. Mol. Biol. **193**, 413 (1987).
[12] M. C. Romano, M. Thiel, I. Stansfield, and C. Grebogi, Phys. Rev. Lett. **102**, 198104 (2009).
[13] T. Chou and G. Lakatos, Phys. Rev. Lett. **93**, 198101 (2004).
[14] J. Dong, B. Schmittmann, and R. Zia, J. Stat. Phys. **128**, 21 (2007).
[15] C. A. Brackley, M. C. Romano, C. Grebogi, and M. Thiel, Phys. Rev. Lett. **105**, 078102 (2010).
[16] D. A. Adams, B. Schmittmann, and R. K. P. Zia, J. Stat. Mech.: Theory Exp. (2008) P06009.
[17] L. J. Cook and R. K. P. Zia, J. Stat. Mech.: Theory Exp.(2009) P02012.
[18] L. J. Cook, R. K. P. Zia, and B. Schmittmann, Phys. Rev. E **80**, 031142 (2009).
[19] A. B. Kolomeisky, G. M. Schütz, E. B. Kolomeisky, and J. P. Straley, J. Phys. A **31**, 6911 (1998).
[20] M. R. Evans, Braz. J. Phys. **30**, 42 (2000).
[21] V. Popkov and G. M. Schutz, EPL **48**, c257 (1999).
[22] M. Ha, J. Timonen, and M. den Nijs, Phys. Rev. E **68**, 056122 (2003).
[23] J. J. Dong, B. Schmittmann, and R. K. P. Zia, Phys. Rev. E **76**, 051113 (2007).
[24] L. B. Shaw, A. B. Kolomeisky, and K. H. Lee, J. Phys. A **37**, 2105 (2004).
[25] G. Tripathy and M. Barma, Phys. Rev. E **58**, 1911 (1998).
[26] L. B. Shaw, J. P. Sethna, and K. H. Lee, Phys. Rev. E **70**, 021901 (2004).
[27] A. B. Kolomeisky, J. Phys. A **31**, 1153 (1998).
[28] Since in steady state the current must be equal through both lattices the MC phase cannot be mixed with other phases. An LD/HD phase cannot be realized for obvious reasons: an LD region cannot be maintained upstream of an HD region since particles would not be able to leave the LD region and the density there would increase.
[29] U. Alon, *An Introduction to Systems Biology*, 1st ed. (Chapman and Hall/CRC, London, 2006).
[30] J. Krug, Phys. Rev. Lett. **67**, 1882 (1991).
[31] From Eq. (9) in the steady state we have $J=(V/L')(\bar{T}-T)/(K_m+\bar{T}-T)$. This has its maximum value when $T=0$; since $K_m \ll \bar{T}$ for realistic parameters, an upper bound for J is therefore V/L'.
[32] F. Borel, C. Vincent, R. Leberman, and M. Hartlein, Nucleic Acids Res. **22**, 2963 (1994).
[33] H. Liu, R. Peterson, J. Kessler, and K. Musier-Forsyth, Nucleic Acids Res. **23**, 165 (1995).
[34] B. Lenhard, S. Filipić, I. Landeka, I. Škrtić, D. Söll, and I. Weygand-Đurašević, J. Biol. Chem. **272**, 1136 (1997).
[35] C. Francklyn, J. Adamd, and J. Augustine, J. Mol. Biol. **280**, 847 (1998).
[36] Q. Zhang, E. Wang, and Y. Wang, Biochim. Biophys. Acta **1387**, 136 (1998).
[37] P. Fechter, J. Rudinger-Thirion, and A. Theobald-Dietrich, Biochemistry **39**, 1725 (2000).
[38] T. von der Haar, BMC Systems Biology **2**, 87 (2008).
[39] Y. Arava, Y. Wang, J. D. Storey, C. L. Liu, P. O. Brown, and D. Herschlag, Proc. Natl. Acad. Sci. U.S.A. **100**, 3889 (2003).
[40] A. B. Bortz, M. H. Kalos, and J. L. Lebowitz, J. Comput. Phys. **17**, 10 (1975).
[41] G. Lakatos and T. Chou, J. Phys. A **36**, 2027 (2003).
[42] L. B. Shaw, R. K. P. Zia, and K. H. Lee, Phys. Rev. E **68**, 021910 (2003).
[43] L. Ciandrini, I. Stansfield, and M. C. Romano, Phys. Rev. E **81**, 051904 (2010).
[44] MATHEMATICA, Wolfram Research, Inc., 2008.
[45] We calculate the roots of the polynomial numerically using the MATHEMATICA [44] function ROOT. Of the six roots only one is physically relevant having real values where $\mathcal{J}_{QP} \to 0$ as $s \to 0$.